# Nanoscale Surface Characterization and Miscibility Study of a Spray-Dried Injectable Polymeric Matrix Consisting of Poly(lactic-co-glycolic acid) and Polyvinylpyrrolidone

JOKE MEEUS,[1] XINYONG CHEN,[2] DAVID J. SCURR,[2] VALERIA CIARNELLI,[2] KATIE AMSSOMS,[3] CLIVE J. ROBERTS,[2] MARTYN C. DAVIES,[2] GUY VAN DEN MOOTER[1]

[1]Pharmacotechnology and Biopharmacy, KU Leuven, Leuven, Belgium

[2]Laboratory of Biophysics and Surface Analysis, School of Pharmacy, The University of Nottingham, NG7 2RD Nottingham, United Kingdom

[3]Pharmaceutical Companies of Johnson & Johnson, Janssen C.R.E.A.Te—Community of Research Excellence and Advanced Technology, ACS, Beerse, Belgium

*Received 31 January 2012; revised 6 February 2012; accepted 2 March 2012*

*Published online 23 March 2012 in Wiley Online Library (wileyonlinelibrary.com). DOI 10.1002/jps.23131*

**ABSTRACT:** Injectable controlled-release formulations are of increasing interest for the treatment of chronic diseases. This study aims to develop and characterize a polymeric matrix for intramuscular or subcutaneous injection, consisting of two biocompatible polymers, particularly suitable for formulating poorly soluble drugs. For this matrix, the water-insoluble polymer poly(lactic-co-glycolic acid) (PLGA) is combined with the water-soluble polymer polyvinylpyrrolidone (PVP). Microparticles of these two polymers were prepared by spray drying. The phase behavior of the samples was studied by means of modulated differential scanning calorimetry and the results showed that phase separation occurred in the bulk sample through evidence of two mixed amorphous phases, namely, a PLGA-rich phase and a PVP-rich phase. Characterization of the samples by scanning electron microscopy demonstrated that the spray-dried particles were hollow with a thin shell. Because of the importance in relation to stability and drug release, information about the surface of the microparticles was collected by different complementary surface analysis techniques. Atomic force microscopy gathered information about the morphology and phase behavior of the microparticle surface. Time-of-flight secondary ion mass spectrometry analysis of the particles revealed that the surface consisted mainly of the PLGA-rich phase. This was confirmed by X-ray photoelectron spectroscopy at an increased sampling depth (~10 nm). Nanothermal analysis proved to be an innovative way to thermally detect the presence of the PLGA-dominated surface layer and the underlying PVP phase. Taken together, this information provides a rational basis for predicting the likely drug release behavior this formulation will display. © 2012 Wiley Periodicals, Inc. and the American Pharmacists Association J Pharm Sci 101:3473–3485, 2012

**Keywords:** PLGA; PVP; microspheres; controlled release; spray drying; DSC; atomic force microscopy; X-ray photoelectron spectroscopy; time-of-flight secondary ion mass spectrometry; nanothermal analysis

## INTRODUCTION

The number of poorly soluble drugs that require formulation into effective medicines has increased steadily during the past two decades. This obviously poses problems not only for oral delivery, but also for the development of injectable formulations, especially in the case of prolonged-release preparations. Baert et al.[1] recently proposed the use of injectable nanosuspensions to sustain the delivery of the anti-HIV drug rilpivirine over several weeks. Despite the success of this strategy, the drawback of this formulation approach is its compound specificity, requiring the need to develop and optimize a formulation for each new

Additional Supporting Information may be found in the online version of this article. Supporting Information

*Correspondence to*: Guy Van den Mooter (Telephone: + 32-16330304; Fax: + 32-16330305; E-mail: guy.vandenmooter@pharm.kuleuven.be)

Journal of Pharmaceutical Sciences, Vol. 101, 3473–3485 (2012)
© 2012 Wiley Periodicals, Inc. and the American Pharmacists Association

chemical entity. Hence, there is a clear need for a more universally applicable delivery platform that enables prolonged release of poorly soluble compounds and would require minimal optimization for different compounds. An ideal drug delivery system should significantly increase effective drug solubility while providing controlled release over an extended period of time (weeks). This study addresses these two hurdles by proposing a novel formulation strategy based on a matrix consisting of the water-insoluble polymer poly(lactic-co-glycolic acid) (PLGA) in combination with the water-soluble polymer polyvinylpyrrolidone (PVP). Each of these polymers has its own function in the formulation. PVP can improve the active pharmaceutical ingredient (API) solubility by facilitating the processing of the API in an amorphous solid dispersion.[2–5] To achieve a meaningful drug load, the miscibility between PVP and the selected API needs to be sufficiently high. The second polymer, PLGA, provides for controlled-release characteristics of the formulation.[6] These characteristics can be influenced by changing the amount of PLGA present in the formulation and/or by adapting the molecular weight of the polymer and/or by using a different ratio of lactic acid to glycolic acid.[7,8] A low miscibility between the PLGA and the selected API as well as a low miscibility between the two polymers is necessary for optimal drug release characteristics. Hence, miscibility behavior, including phase behavior as well as phase distribution, of the different compounds is a key characteristic and justification for the study presented in this paper.

The two polymers were selected based upon their differences in solubility and their biocompatibility, a characteristic which only applies to a limited number of polymers. Both PLGA and PVP are already used individually as a matrix material in commercial drug products. Examples include Cesamet® (Valeant Pharmaceuticals Inc. Costa Mesa, California) and Rezulin® (Warner-Lambert Co. Morris Plains, New Jersey), using PVP as a carrier,[2,4] and Trelstar® Depot (Debio RP, Martigny, Switzerland),[9] Sandostatin LAR® (Novartis Pharmaceuticals, East Hanover, New Jersey),[10] and Risperdal® Consta® (Janssen Pharmaceutica, Beerse, Belgium),[11] using PLGA as a carrier. A combination of these polymers has not been reported, indicating the novelty and scope of the present study.

The combined PLGA–PVP microparticles were prepared by spray drying and investigated in terms of polymer mixing behavior and surface characteristics, as well as the influence of the ratio of PLGA–PVP on these characteristics. A combination of several complementary solid-state characterization techniques was applied. Modulated differential scanning calorimetry (MDSC) was used to study whether PLGA and PVP showed the desirable phase behavior, that is, immiscibility. Nanoscale surface characteristics of the microparticles were analyzed using atomic force microscopy (AFM)[12–14] for studying the morphology and phase behavior, time-of-flight secondary ion mass spectrometry (ToF-SIMS)[15,16] and X-ray photoelectron spectroscopy (XPS)[12,15] for surface chemical quantification, and nanothermal analysis (nanoTA)[14,17,18] for local thermal surface characterization. NanoTA on binary polymeric particles has not been reported yet, and the results obtained in this study demonstrate the applicability of this technique for this type of sample geometry.

An understanding of the surface behavior will form the basis for the rational development of a drug matrix with desired and tuneable characteristics in terms of drug solubility enhancement and drug release profile in a later stage of research. The outcome of this study will have implications for the development of the polymeric drug matrix to deliver the optimum-release properties for poorly soluble drugs in future studies.

## EXPERIMENTAL SECTION

### Materials

Polyvinylpyrrolidone K30 (PVP K30) (molecular weight 44–54 kDa) was kindly donated by BASF (Ludwigshafen, Germany). PLGA (lactide–glycolide molar ratio of 75:25, inherent viscosity of 0.2 dL/g) was purchased from PURAC Biomaterials (Gorinchem, The Netherlands).

### Methods

#### *Spray Drying*

Spray-dried samples were prepared with a Micro Spray laboratory-scale spray dryer (ProCepT, Zelzate, Belgium). A 15% feed solution of the polymers in dichloromethane was used. The inlet temperature was set to 95°C and the feed rate was 6 mL/min. The cocurrent drying air had a flow rate of 0.2 $m^3$/min, and the atomizing air was supplied with a pressure of 5 bar.

#### *Physical Mixtures*

Physical mixtures of the amorphous spray-dried bulk polymers PLGA and PVP K30 were prepared according to the rules of geometrical blending using a mortar and pestle.

#### *Modulated Differential Scanning Calorimetry*

Bulk miscibility of the samples was analyzed by MDSC (Q2000; TA Instruments, Leatherhead, UK). The data obtained were analyzed with the Thermal Analysis Software (version 4.4A) (TA Instruments, Leatherhead, UK). Crimped aluminum pans (TA Instruments, Brussels, Belgium) were used for the

analysis of the samples. An empty pan was used as a reference and the masses of the reference pan and of the sample pans were taken into account. The DSC cell was purged with a nitrogen flow at a flow rate of 50 mL/min.

Temperature calibration was performed using indium and octadecane. Calibration of the enthalpic response was performed with indium. The modulation parameters used were: a heating rate of 1°C/min, a period of 40 s, and an amplitude of 1°C. Calibration of the heat capacity was performed using sapphire. Samples were analyzed from −20°C to 220°C. Glass transitions ($T_g$s) were analyzed in the reversing heat flow signals.

### Scanning Electron Microscopy

Samples were prepared by fixing an amount of powder on an aluminum stub using double-sided carbon tape. The samples were gold coated by sputtering with gold for 45 s at 20 mA. Field emission gun scanning electron micrography (FEG-SEM) images were taken by using a Philips XL30 ESEM-FEG instrument (Philips, Eindhoven, The Netherlands) at an acceleration voltage of 10 kV.

### Atomic Force Microscopy

An EnviroScope Atomic Force Microscope (BrukerNano, Cambridge, UK) was used for the AFM experiments. Measurements were conducted at a temperature of 25°C and a relative humidity of 20%. Commercial silicon AFM tips were used (BrukerNano) with spring constants from 20 to 80 N/m and resonance frequencies between 347 and 393 kHz. Mica slides (Agar Scientific, Stansted, UK) were used as sample substrate. Gwyddion software (version 2.22) (Czech Metrology Institute, Brno, Czech Republic) was used for image analysis.

### Time-of-Flight Secondary Ion Mass Spectrometry

Spray-dried samples were adhered to double-sided tape to produce an immobile surface suitable for ToF-SIMS analysis. The data were acquired using a ToF-SIMS IV instrument (ION-TOF GmbH, Münster, Germany) equipped with a bismuth liquid metal ion gun and a single-stage reflectron analyzer. Typical operating conditions utilized a $Bi_3^+$ primary ion energy of 25 kV and a pulsed target current of approximately 1.0 pA. A flood gun producing low-energy electrons (20 eV) was used to compensate for surface charging caused by the positively charged primary ion beam on the insulating sample surface. Each sample was raster scanned at a resolution of 256 × 256 pixels. By keeping the total primary ion beam dose for every analyzed area below $1 \times 10^{12}$ ions/cm$^2$ throughout the analysis, static conditions were ensured. Data in the negative secondary ion polarities were collected and analyzed using SurfaceLab 6 (ION-TOF Gmbh, Münster, Germany). PLGA and PVP were identified using $C_2HO_3^-$ ($m/z$ = 73), and $CN^-$ + $CNO^-$ ($m/z$ = 26 and 42, respectively). Beforehand reference samples were analyzed and the characteristic peaks, $CN^-$, $CNO^-$, and $C_2HO_3^-$, were selected and only present in the appropriate samples.

For the sputtering procedure, a $C_{60}^+$ ion gun was used to remove multiple layers of material between analytical cycles. The total number of sputter cycles depended on the sample composition. For these experiments, a 200 pA target current and a sputter time of 7 s were used.

The imaged data were all acquired using the "burst alignment" setting on the instrument to achieve the high spatial resolution (~200 nm) required to resolve individual particles.

### X-Ray Photoelectron Spectroscopy

X-ray photoelectron spectroscopy analysis was performed by using a Kratos Axis Ultra instrument (Kratos Analytic, Manchester, UK) equipped with a monochromated Al Kα X-ray source (1486.6 eV), employing hybrid (magnetic/electrostatic) optics, a hemispherical analyzer, a multichannel plate, a delay line detector with collection and takeoff angles of 30° and 90°, respectively. The instrument was operated at 15 mA emission current and 10 kV anode potential. Again, spray-dried samples were adhered to double-sided tape. Wide scans were run for 5–10 min at three different positions on the powder surface, with an analysis area of 0.3 × 0.7 mm$^2$. The instrument was run using the CASAXPS software (version 2.3.16) (Casa software ltd, Teignmouth, United Kingdom). High-energy resolution C 1s, N 1s, O 1s, and Si 2p spectra were obtained. Charge neutralization was accomplished during analysis using a flood gun.

Survey scans were accomplished using a pass energy of 80 eV, a step size of 1 eV, and an acquisition time of 10 min. High-resolution scans were obtained using a pass energy of 20 eV, a step size of 0.1 eV, and an acquisition time of 5 min.

### Nanothermal Analysis

A multimode nanoscope IIIa (BrukerNano) equipped with a nanoTA module and a nanoTA probe (Anasys Instruments, Santa Barbara, California) was used to perform nanoTA. Data were acquired in contact mode. To determine the location where nanoTA would be conducted, a tapping mode AFM image was first obtained to visualize the selected area. Subsequently, a location was chosen where the thermal analysis was performed with oscillation amplitude turned to zero. Commercial AN2-200 nanoTA probes were used (Anasys Instruments) with spring constants from 0.5 to 3 N/m and resonance frequencies between 55 and 80 kHz. The probes were heated at a controlled rate of 1°C/s. Temperature calibration of the probes was

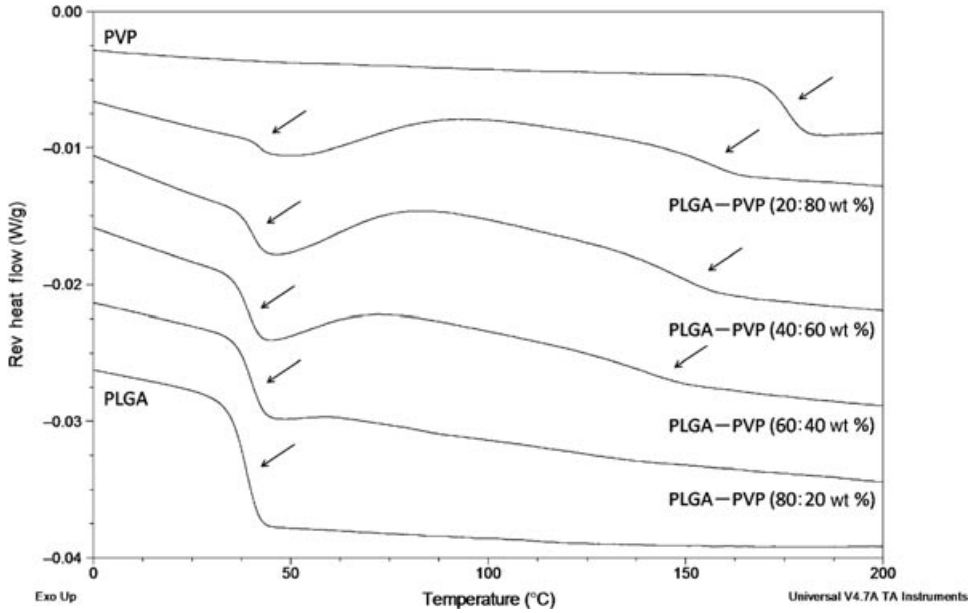


**Figure 1.** MDSC of spray-dried PLGA–PVP mixtures. From top to bottom: reversing heat flow of PVP, PLGA–PVP 20:80 (wt %), 40:60 (wt %), 80:20 (wt %), and PLGA. The arrows indicate the $T_g$ temperatures.

obtained by using three polymers with known melting temperature, namely, polycaprolactone ($T_m = 55°C$), polyethylene ($T_m = 116°C$), and polyethyleneterephthalate ($T_m = 235°C$). During the experiments, the deflection of the cantilever is recorded in function of the temperature of the tip, in which thermal events such as melting or a $T_g$ can be revealed.

## RESULTS

### Bulk Sample Characterization

#### *Miscibility of PVP and PLGA in the Spray-Dried Particles*

The phase behavior of PVP K30 and PLGA in spray-dried particles was studied by MDSC. The ratio of PLGA to PVP was 20:80, 40:60, 60:40, and 80:20 (wt %). Two $T_g$s are observed in the reversing heat flow curves of the spray-dried mixtures indicating phase separation (Fig. 1). The obtained $T_g$ values do not correspond to the $T_g$s of the pure compounds (around 39°C for PLGA and 174°C for PVP), but are shifted toward each other, resulting in two mixing $T_g$s.

Physical mixtures consisting of the same polymer ratios were used to verify whether the in-phase miscibility (the mixing of a small amount of PVP in the PLGA phase or vice versa) occurred during the spray drying process or resulted from the MDSC run due to the slow underlying heating rate. The results for the spray-dried samples and the physical mixtures were compared and, in contrast to the spray-dried samples, the physical mixtures had the $T_g$s of the pure polymers. For an overview of the exact values of the measured $T_g$s, the reader is referred to Table 1 of the Supporting Information.

On the basis of the mixing $T_g$s observed in the thermograms, the theoretical amounts of PVP present in the PLGA-rich phase (based upon $T_{g1}$, the first $T_g$ observed in the thermograms) and of PLGA present in the PVP-rich phase (based upon $T_{g2}$, the second $T_g$ observed in the thermograms) were estimated by means

**Table 1.** Theoretical Atomic Compositions as Percentages and Experimental Atomic Compositions as Percentages ± SD for the C 1s, O 1s, and N 1s Spectra of the Spray-Dried Samples

| | Theoretical Atomic Composition (%) | | | Experimental Atomic Composition (%) | | |
|---|---|---|---|---|---|---|
| Sample ID | C 1s | O 1s | N 1s | C 1s | O 1s | N 1s |
| Pure | | | | | | |
| PLGA | 57.9 | 42.1 | – | 64.8 ± 0.4 | 35.2 ± 0.4 | – |
| PVP | 75.0 | 12.5 | 12.5 | 78.4 ± 0.5 | 10.5 ± 0.2 | 11.1 ± 0.5 |
| PLGA–PVP (wt %) | | | | | | |
| 20/80 | 71.6 | 18.3 | 10.0 | 68.3 ± 0.4 | 27.2 ± 0.3 | 2.9 ± 0.3 |
| 40/60 | 68.2 | 24.2 | 7.6 | 65.0 ± 0.5 | 34.2 ± 0.6 | 0.8 ± 0.2 |
| 80/20 | 64.8 | 30.1 | 5.1 | 64.9 ± 0.8 | 35.1 ± 0.8 | – |

The SD is calculated for four different positions on each sample.

**Table 2.** Percentage of PVP Present in the PLGA-Rich Phase (Based Upon $T_{g1}$, the first $T_g$ Observed in the Thermograms) and of PLGA in the PVP Phase (Based Upon $T_{g2}$, the First $T_g$ Observed in the Thermograms) Calculated by Means of the Gordon–Taylor Equation

| | First Mixing $T_g$: PLGA-Rich Phase | | Second Mixing $T_g$: PVP-Rich Phase | |
|---|---|---|---|---|
| Sample Composition (PLGA/PVP wt %) | PLGA Present (%) | PVP Present (%) | PLGA Present (%) | PVP Present (%) |
| 20:80 | 91.0 | 9.0 | 3.6 | 96.4 |
| 40:60 | 95.9 | 4.1 | 5.2 | 94.8 |
| 60:40 | 99.1 | 0.9 | 7.8 | 92.2 |
| 80:20 | 98.2 | 1.8 | 8.3 | 91.7 |

of the Gordon–Taylor equation (Eq. 1).

$$Tg_{mix} = \frac{(w_1 Tg_1 + \mathrm{K}w_2 Tg_2)}{(w_1 + \mathrm{K}w_2)} \quad (1)$$

In Eq. 1, the weight fraction of each compound is represented by $w$, the glass transition by $T_g$, and the subscripts 1 and 2 represent, respectively, the compounds with the lowest and the highest glass transition temperatures. The constant $K$ can be assessed by using the Simha–Boyer rule (Eq. 2), with $\rho$ being the density of the amorphous compounds.

$$K \cong \frac{\rho_1 Tg_1}{\rho_2 Tg_2} \quad (2)$$

The calculated fractions are shown in Table 2 of the Supporting Information.

### *Morphology of the Spray-Dried Particles*

Scanning electron microscopy was used to study the morphology of the spray-dried microparticles (Fig. 2). It was observed that the spray-dried particles were hollow with a thin shell (Fig. 2d). SEM images also revealed that particle size varied mainly between 2 and 20 μm, and depending on the polymer ratio of the samples, some tendencies with relation to particle shape and smoothness of the particle surface were observed (Figs. 2a–2f). Particles obtained by spray drying a feed solution containing only PVP were observed in a scanning electron microscope to be mainly irregularly shaped and collapsed particles, although with a smooth surface, but spherical particles were also detected (Fig. 2a). When a PLGA solution was spray dried, the obtained particles were more regular and spherical in shape (Fig. 2b). These characteristics can still be recognized in the samples with varying PLGA–PVP ratios (Figs. 2c–2f). For example, it can be seen that the PLGA–PVP 20:80 (wt %) sample resembles the pure PVP sample because of its high PVP content (Fig. 2c). The opposite is true for the PLGA–PVP 80:20 (wt %) sample; here, the same spherically shaped particle morphology can be detected as for the pure PLGA sample (Fig. 2f).

## Surface Characterization of the Spray-Dried Particles

### *Topographic and Mechanical Surface Characterization*

Nanoscale information about the surface topography and mechanical behavior was obtained by tapping mode AFM. Height images of the samples provide topographical information about the sample surface. Phase images reveal spatial material and chemical heterogeneities in a sample through variation in the tip–sample interactions.[19] On the basis of the obtained height images, a variation in surface topography was observed among different samples and even among different particles from the same sample (Figs. 3a–3c). The height differences on most of the particle surfaces are limited to the range of some 20 nm over image sizes of up to $5 \times 5\,\mu m^2$. Larger differences in height were observed when the surface was locally damaged, as shown in Figures 3d and 3e. Here, the phase image shows the presence of a second phase at the surface. Interestingly, inspection of the same area of the corresponding height image shows a topographic feature at the same position in the scanned area (see inset).

### *Chemical Surface Characterization*

*Time-of-Flight Secondary Ion Mass Spectrometry Surface Analysis.* Two complementary techniques were used to analyze the chemical composition of the surface. On the basis of the detection of molecular fragments, ToF-SIMS analysis typically provides information about the chemical composition of the first surface monolayer of a sample, whereas the information on atomic concentrations and chemical bonding obtained with XPS covers an increased sampling depth (ca. 10 nm).

Because of the relatively high spatial resolution of ToF-SIMS (~1 μm for a $250 \times 250\ \mu m^2$ area and 250 nm for a $60 \times 60\,\mu m^2$ area), it was possible to image the sample surface through high-resolution intensity maps, as shown in Figure 4. In these data, colors can be made to correspond to specific mass fragments and hence polymer. Individual particles could be clearly distinguished. The negative polarity overlay images, where PLGA is displayed in green and PVP in red, reveal that the surface consisted mainly of PLGA. Occasionally, red spots indicating the

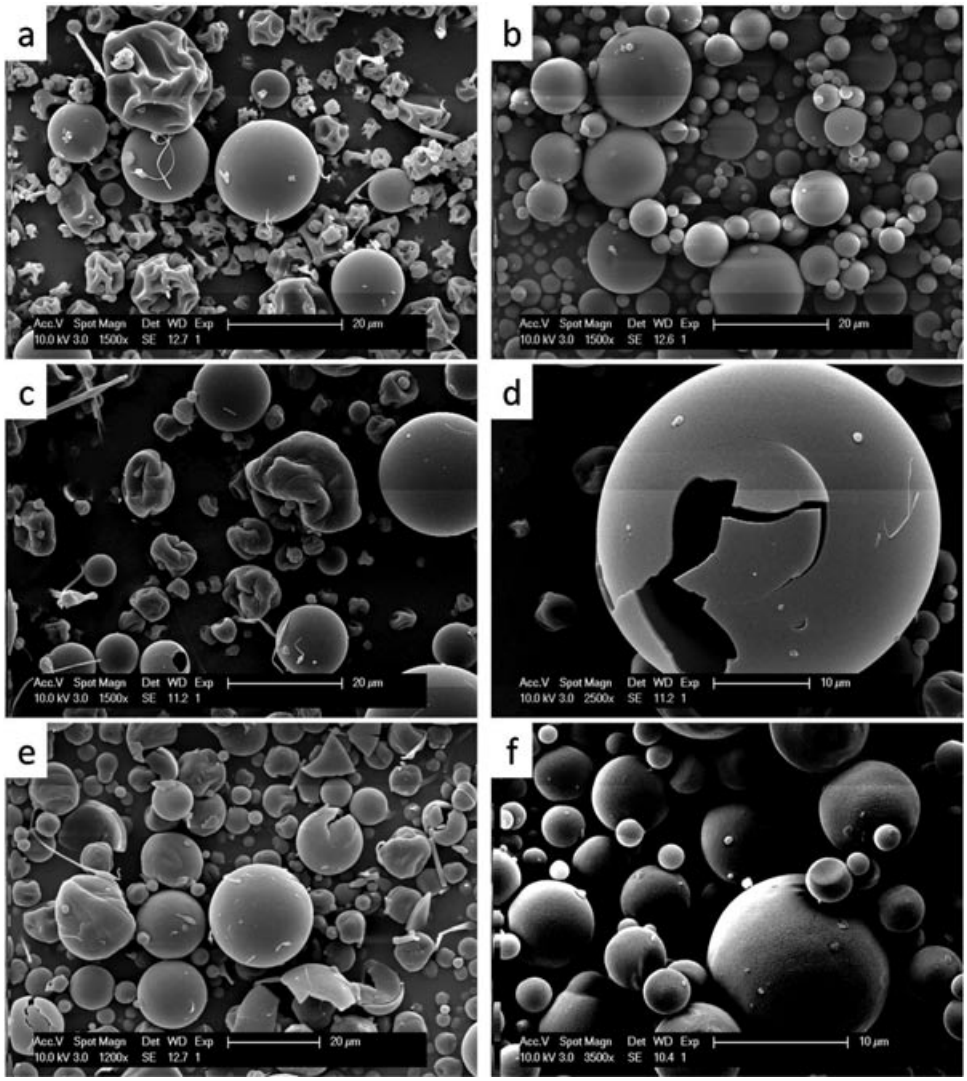


**Figure 2.** Scanning electron micrographs of spray-dried materials. (a) PVP K30, (b) PLGA, (c) and (d) PLGA–PVP 20:80 (wt %), (e) PLGA–PVP 40:60 (wt %), and (f) PLGA–PVP 80:20 (wt %).

presence of PVP were observed. In Figures 4e–4h, where only one particle is imaged, a high-intensity spot is observed in the negative polarity image of PVP (Fig. 4f, indicated by the arrow). When comparing the same area on the negative polarity image of PLGA (Fig. 4g), a low-intensity area can be observed. The overlay image shows that this red PVP area is surrounded by a green PLGA area without an overlap of the two phases (Fig. 4h). This implies that there is either predominantly PLGA or PVP present at the surface, but not a mixture of both within the sensitivity limits of Tof-SIMS imaging.

*ToF-SIMS Depth Analysis Using $C_{60}^+$ Sputtering.* A $C_{60}^+$ beam was used to sputter the sample surface to remove the first few monolayers; hence, fresh surfaces were revealed for ToF-SIMS analysis and were scanned again using the $Bi_3^+$ primary ion source to collect information about the chemical composition (Fig. 5). The size of sample area exposed to the $C_{60}^+$ sputter beam was set slightly smaller than the imaged area, so that the margins of the images show the spray-dried material in its original condition. This makes it convenient for comparison with the sputtered area (sputtered area: $400 \times 400\,\mu m^2$, imaged area: $500 \times 500\,\mu m^2$). After the first sputter cycle, for both the PLGA–PVP 20:80 (wt %) sample and the 40:60 (wt %) sample, a clear increase in the presence of PVP at the surface was observed. In addition, the intensity of the PVP signal is clearly higher for the PLGA–PVP 20:80 (wt %) sample because of its higher PVP content. Considering the 20:80 (wt %) PLGA–PVP sample, it was observed that the intensity signal from PVP hardly increases with more sputter cycles. In case of the 40:60 (wt %) PLGA–PVP sample, more sputter cycles are necessary to increase the PVP

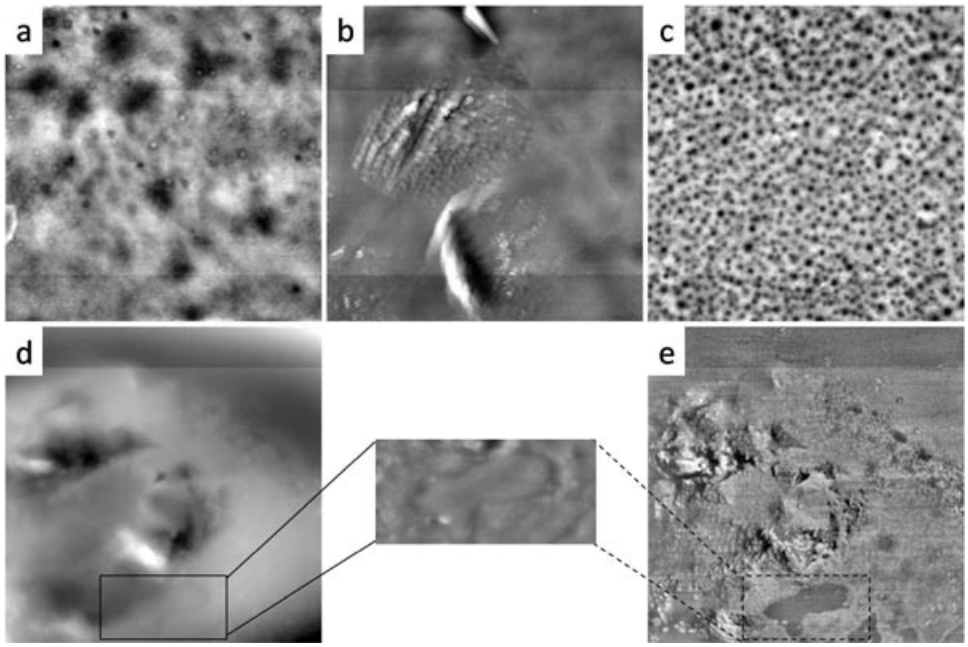


**Figure 3.** Atomic force micrographs. (a) and (b) PLGA–PVP 40:60 (wt %) (height image, $4 \times 4\,\mu m^2$ scan size), (c) PLGA–PVP 20:80 (wt %) (height image, $4 \times 4\,\mu m^2$ scan size), (d) PLGA–PVP 40:60 (wt %) (height image, $5 \times 5\,\mu m^2$ scan size), and (e) PLGA–PVP 40:60 (wt %) (phase image, $5 \times 5\,\mu m^2$ scan size). Inset (height image): $2 \times 1\,\mu m^2$ scan size.

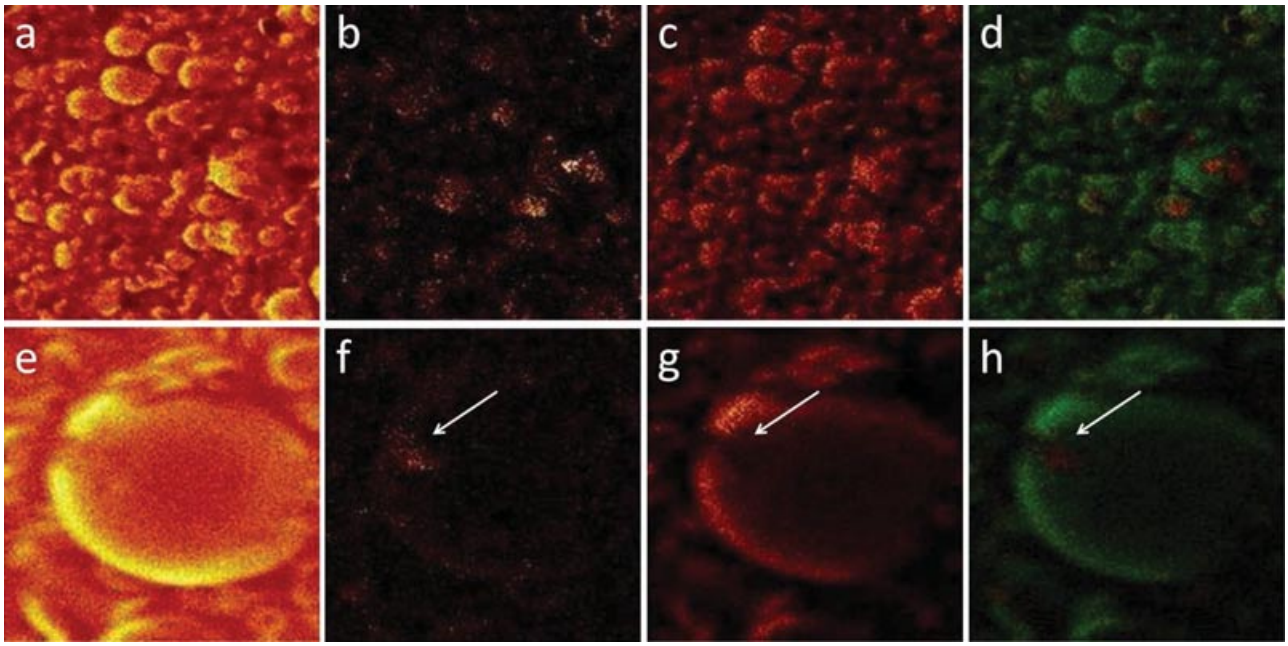


**Figure 4.** ToF-SIMS intensity maps of a PLGA–PVP 40:60 (wt %) sample. Panels (a)–(d) show images of a scan area of $250 \times 250\,\mu m^2$. Panels (e)–(h) have a $60 \times 60\,\mu m^2$ scan area. Panels (a) and (e) show results of the total intensity signal. Panels (b) and (f) show negative polarity images of $CN^-$ and $CNO^-$ (PVP). Panels (c) and (g) show negative polarity images of $C_2HO_3^-$ (PLGA). Panels (d) and (h) show the negative polarity overlay images (PVP in red, PLGA in green).

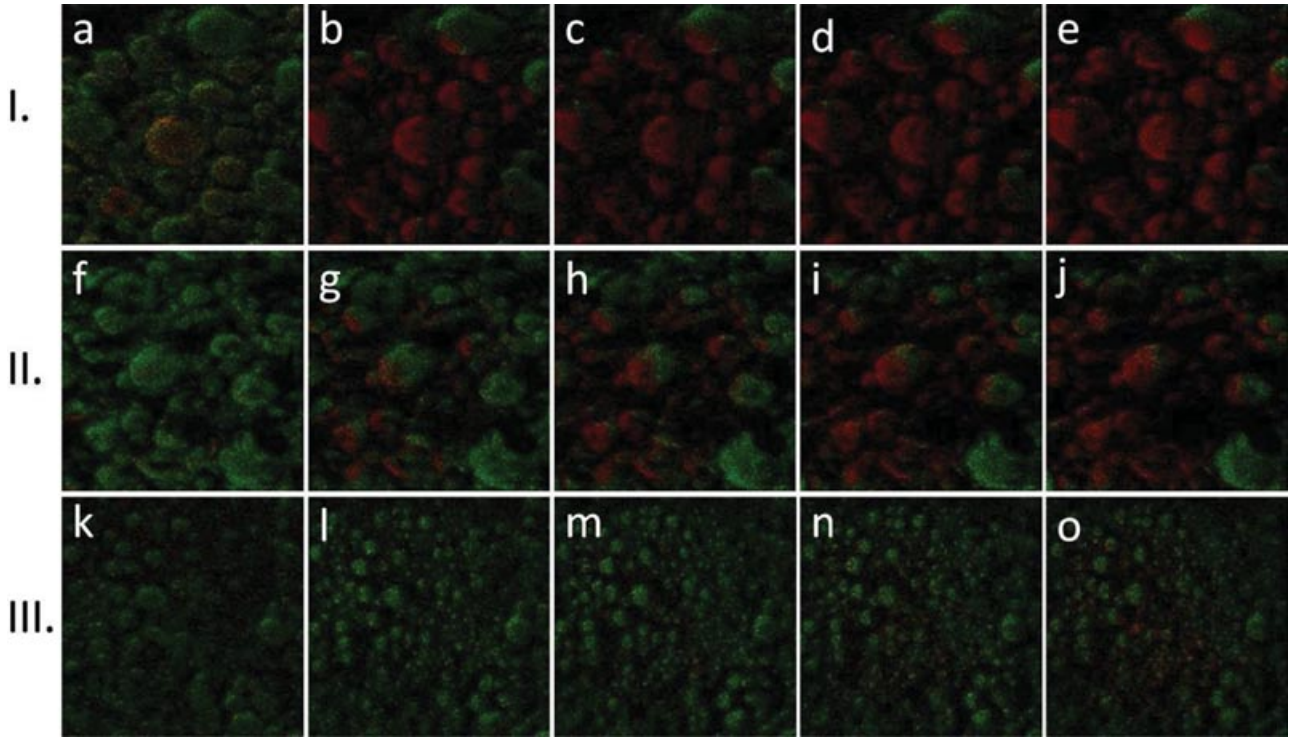


**Figure 5.** Negative polarity overlay images after $C_{60}^+$ sputtering of different samples (200 × 200 $\mu m^2$ scan size). I, PLGA–PVP 20:80 (wt %); II, PLGA–PVP 40:60 (wt %); and III, PLGA–PVP 80:20 (wt %). (a) The original sample surface, (b) the surface after one sputter cycle, (c) the surface after a second sputter cycle, (d) the surface after a third sputter cycle, and (e) the surface after a fourth sputter cycle. Analogical for rows II and III. PVP is displayed in red, whereas PLGA in green.

intensity signal to a comparable level. For the sample consisting of 80 (wt %) PLGA, it was seen that within the same number of sputter cycles, the PVP intensity signal does not increase significantly.

*X-Ray Photoelectron Spectroscopy.* Complementary to the ToF-SIMS experiments, XPS was performed. The peak in the XPS spectra associated with nitrogen was used as the diagnostic peak for the presence of PVP (not present in PLGA). The quantification of the oxygen peak gave an indication about the presence of PLGA because of the higher fraction of oxygen present in the molecular structure of PLGA compared with PVP. It should be kept in mind that the oxygen signal does not exclusively contain information about PLGA, considering the fact that PVP also contains oxygen atoms, although relatively less. High-resolution scans of the C 1s peak show that the PLGA–PVP mixtures possess the characteristic carbon bonds present in both the pure polymers (Fig. 1 of the Supporting Information).

Table 1 displays the theoretical atomic percentages and the experimentally obtained values. When comparing these values, it can be observed that for the different PLGA/PVP samples, the experimental nitrogen concentrations (hence the PVP concentrations) are lower than expected. The nitrogen concentration increases with PVP content in the PLGA–PVP samples, although it is still lower than the theoretically expected concentration.

Another noticeable observation was the higher experimental atomic carbon concentration for PLGA compared with the theoretical value. A value of 64.8% was noted instead of the expected 57.9%.

When reviewing the C 1s spectrum for spray-dried PLGA particles, a higher experimental atomic carbon concentration coming from the C—C bond of PLGA (38.18%, with a standard deviation of 2.83) was revealed, compared with the theoretical value for the pure polymer (33.33%).

### *Thermal Surface Characterization*

Nanothermal analysis was used to thermally characterize the surface of the microparticles. For this technique, a sudden change in deflection of the heated cantilever indicates a thermal transition of the sample surface, and in this case, it marks the $T_g$ temperature of the examined surface region.

The results for the pure polymers are shown in Figure 6 (curves I and III). The surface $T_g$s of PLGA and PVP were observed at around 47°C and 155°C, respectively, comparable to values of around 39°C and

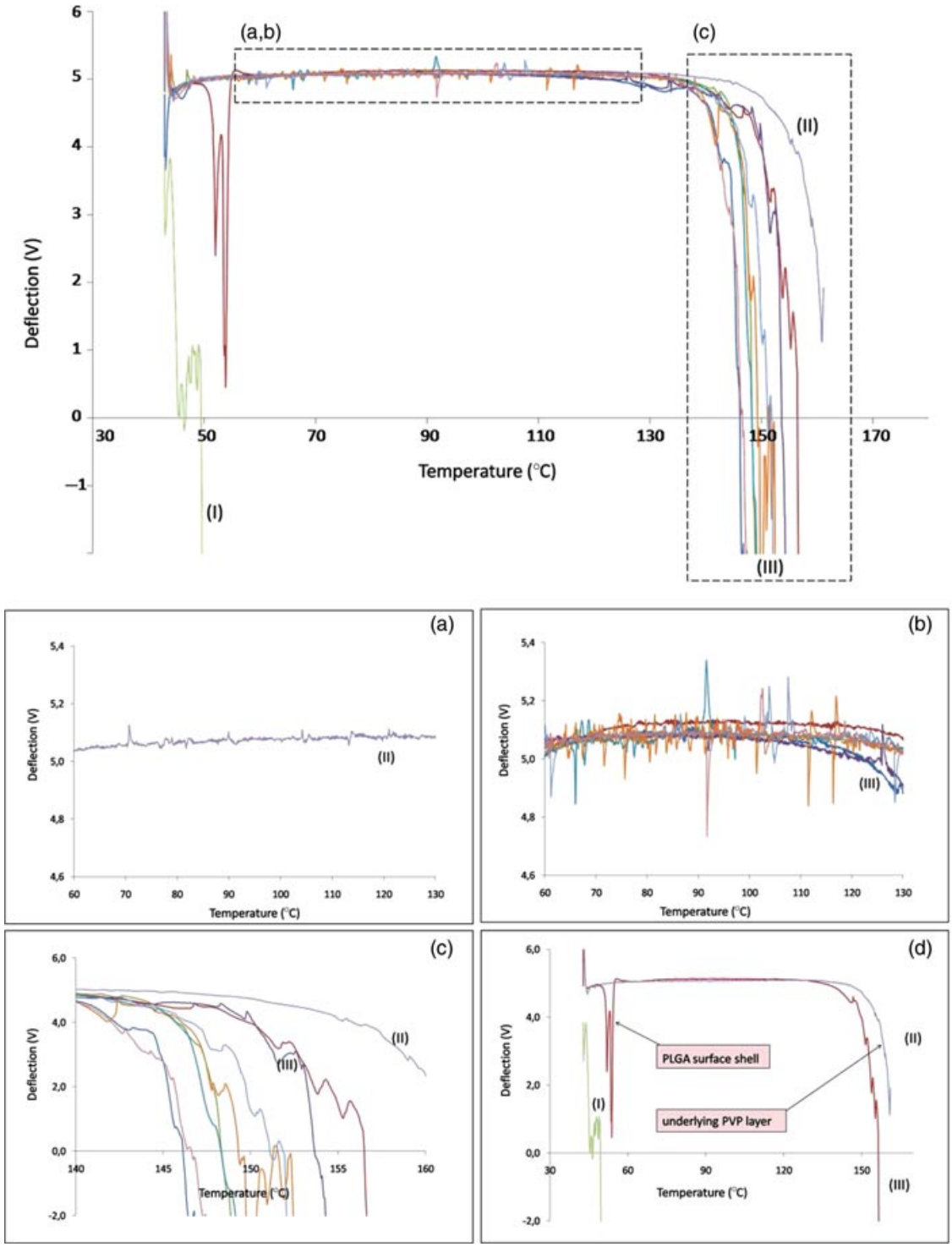


**Figure 6.** nanoTA data of PLGA (curve I), PLGA–PVP 40:60 (wt %) (curves II), and PVP (curve III) samples. Inset (a) displays the baseline of PVP. Inset (b) displays the baseline of the PLGA–PVP samples. Inset (c) shows an enlarged view on the transition of the PLGA–PVP samples and PVP itself. Inset (d) displays the pure polymers and a PLGA–PVP sample possessing two transitions.

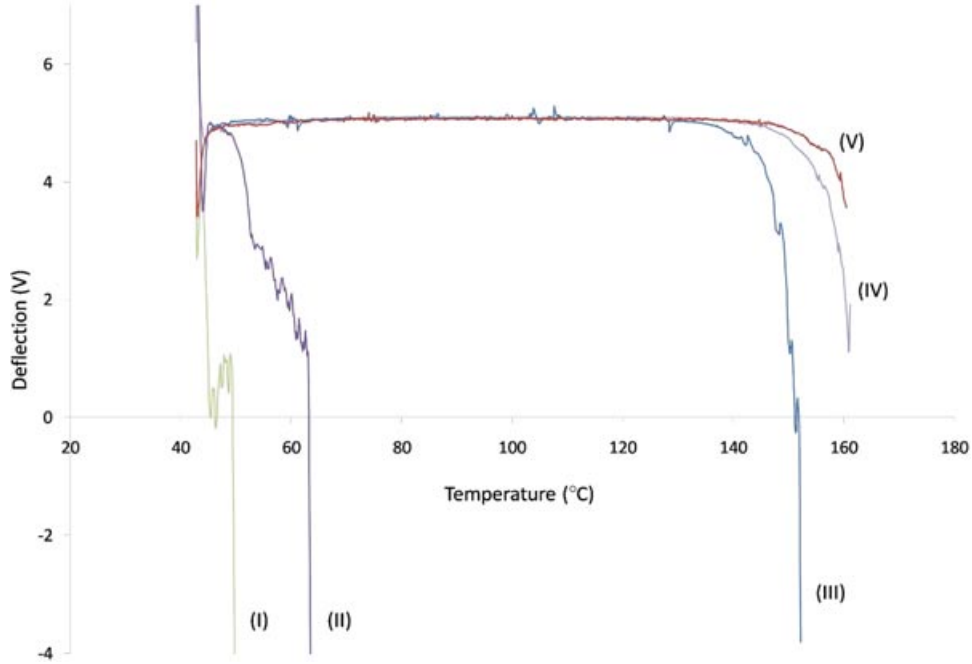


**Figure 7.** nanoTA data of PLGA (curve I), PLGA–PVP 80:20 (wt %) (curve II), PLGA–PVP 40:60 (wt %) (curve III), PLGA–PVP 20:80 (wt %) (curve V), and PVP (curve IV).

174°C from MDSC analysis of the bulk polymers. Note that this temperature variation between the two techniques is generally considered to relate to the large difference in heating rate (1°C/s for nanoTA compared with 1°C/min for DSC), the difference in analysis method, and the difference between measuring at a small local spot (~10 to 100 s nm in diameter) at the sample surface versus bulk measurements.[20] Furthermore, it should also be noted that nanoTA detects softening of a material under the heated probe, indicated by penetration of the probe into the material. The temperature at which this occurs (the softening point) is indicative for approaching the $T_g$, but does not necessarily exactly corresponds to it.

In Figure 6, curve II displays the results for measurements from different particles of a PLGA–PVP 40:60 (wt %) sample. Figure 6d displays the results for a particle with a PLGA–PVP 40:60 (wt %) composition possessing two transitions: the first transition, around 55°C, marks the detection of the PLGA surface shell and the second at around 150°C represents the underlying PVP phase. It is observed for the PLGA–PVP samples that they lack a distinctive event marking the presence of the PLGA shell and have more noise in the baseline (Fig. 6b) in comparison with the pure polymers (Fig. 6a). Figure 6c demonstrates that there is also more noise detected during the temperature transition of the underlying PVP phase when comparing the samples with the pure polymer.

An overview of results for particles consisting of different polymer ratios [PLGA–PVP 20:80, 40:60, and 80:20 (wt %)] is given in Figure 7. The samples consisting of 80 (wt %) PVP showed a $T_g$ close to that one of the pure PVP polymer. Samples containing 40 (wt %) PLGA showed, as previously mentioned, one or two transitions: a $T_g$ belonging to the PLGA phase and/or a $T_g$ representing the PVP-rich phase. Samples composed of 80 (wt %) PLGA and only 20 (wt %) PVP showed a transition temperature approximately 10°C higher than the $T_g$ of pure PLGA.

## DISCUSSION

The mixing $T_g$s observed in the thermograms (Fig. 1) indicate the presence of two mixed amorphous phases: a PLGA-rich phase and a PVP-rich phase. The amount of PVP present in the PLGA-rich phase and vice versa was estimated from the observed $T_g$s using the Gordon–Taylor equation (Table 2 of the Supporting Information). The results demonstrate that, depending on the PLGA–PVP ratio, the mixed polymer phase represented by the first $T_g$ in each thermogram was estimated to contain at least 91% PLGA and therefore this phase will be named the PLGA-rich phase from here on. The second mixed polymer phase, represented by the second $T_g$ in the thermograms, was calculated to contain at least 91% PVP, depending again on the PLGA–PVP ratio of the feed solution and consequently will be called the PVP-rich phase.

On the basis of these MDSC results, it is stated that depending on the ratio of PLGA and PVP in the feed solution, different polymer phases can be present: a

PLGA-rich phase containing some PVP and a PVP-rich phase containing some PLGA.

The values for the first and second $T_g$ (Table 1 of the Supporting Information) remained fairly constant for the physical mixtures, proving that the in-phase miscibility can be assigned to the spray drying process and is not induced by the MDSC experiment.

The appearance of hollow, shell-structured microparticles after spray drying (Fig. 2) indicates that during the evaporation process, the diffusional motion of the polymer is not sufficiently fast to allow shrinkage of the droplet surface. This results in an enrichment of the polymer at the droplet surface, followed by shell formation. This phenomenon is related to the ratio of the evaporation rate and the diffusion coefficient of the compound, which is represented as the Peclet number (*Pe*) (Eq. 3).[21] In this case, the *Pe* will be greater than one.

$$Pe_i = \frac{\mathrm{K}}{8D_i} \tag{3}$$

In Eq. 3, the evaporation rate is represented by $K$ and $D_i$ stands for the diffusion coefficient of solute $i$.

Particle morphology may be related to the PLGA–PVP ratio in the spray-dried particles (Fig. 2): particle sphericity increased with increasing PLGA content, an increasing PVP content resulted in more irregularly shaped and collapsed particles.

The topographic interparticle variation (Fig. 3) is inherent to the variation in droplet formation and individual drying kinetics during the spray drying process.

Figure 3b shows what are proposed to be "footprints" caused by interparticle collisions during the spray drying process. Support for this hypothesis can be found in previous SEM images (Fig. 2) where it can be observed that collision between large and small particles is a frequently occurring event.

Unusual height differences associated with cracks and other surface damage, caused by particle–particle and particle–wall collisions during the spray drying process, and particle rupture due to solvent evaporation are apparent in the AFM (Fig. 3) and SEM images (Fig. 2). As the AFM phase image (Fig. 3e) shows the presence of a second material phase at the surface and a topographic change is detected at the same area, it is hypothesized that, at this location, the surface layer is removed because of particle damage and as a consequence, a second underlying material phase is detected. This hypothesis is supported by the ToF-SIMS and XPS data.

The findings in Figure 4 are in agreement with the MDSC data, which already indicated that the two polymers were not present as one mixed phase, but were to an extent phase separated. Note that the MDSC experiments revealed that this is in fact a PLGA-rich phase containing a small amount of PVP and vice versa.

Two questions arise from these results, the first one being "Why is PLGA predominantly present at the surface?" To answer this question, and with the knowledge that PVP is not surface active,[22,23] a proof of surface activity of PLGA needs to be provided. This evidence was found in the literature, where different research groups have reported surface segregation of apolar side groups at a polymer–air interface, including nonpolar methyl side groups as present in PLGA.[24–26] A study performed by Thanki et al.[27] reports on this phenomenon in PLGA films, where they observed a surface segregation and surface restructuring of the methyl side groups. It is proposed that the same mechanism of surface restructuring occurs in the spray-dried particles and accounts for the predominant presence of PLGA at the particle surface.

The second question is "What is the reason that on certain, limited areas of the particle surface we observe a PVP signal instead of the predominantly present PLGA surface layer?" To answer this question, the reader is referred to the data in Figures 3d and 3e, where the same irregularly shaped structure in the AFM height image and in the phase image was detected. This observation in combination with the ToF-SIMS data suggests that the particles are mainly covered by a PLGA-rich surface layer, with an underlying PVP-rich layer, which can appear at the surface in case of surface damage and therefore be detected. Collision of particles during the spray drying process is most probably responsible for the surface damage on the individual particles. During spray drying, there is a high probability for the particles formed to be exposed to collisions before and after formation of the final structure on their way from the drying chamber to the collection recipient. Collision can occur among different particles; between particles and the wall of the drying chamber, when transported through the glass connection from the drying chamber to the cyclone; and finally, in the sample collection recipient, when being collected using a tangential vortex. Susceptibility of the particles to damage caused by collision depends on multiple factors such as the elastic and plastic characteristics of the material and brittleness of the formed particles.

The depth profiling ToF-SIMS sputter experiment was performed to confirm the hypothesis of a PLGA surface layer on PVP. This showed a clear relation between the PVP intensity signal after one sputter cycle and the total PVP content of the sample. The amount of sputter cycles (and hence surface material removed) necessary to reveal a maximum PVP intensity signal of the sample indicates the thickness of the covering PLGA surface layer. For example, the high PVP intensity signal after the first sputter cycle for the PLGA–PVP 20:80 (wt %) sample implies that, for

this sample, the surface PLGA layer is, at least partially, removed and the underlying PVP layer becomes detectable. The fact that for the PLGA–PVP 40:60 (wt %) sample three more sputter cycles were necessary to increase the PVP intensity signal to a comparable level indicates a thicker PLGA surface layer compared with the 20:80 PLGA–PVP (wt %) sample, consistent with a higher percentage of PLGA in this sample.

These findings have implications for the development of this polymeric drug matrix to deliver the optimum drug release properties in future studies, namely, the fact that PLGA is located on the surface of the microspheres indicates good potential for controlled release from the underlying drug-rich PVP layer: as the PLGA layer thickness can be tuned, so can the release characteristics.

The XPS data in Table 1 show lower nitrogen concentrations compared with the theoretically expected ones (from the bulk polymer ratio), consistent with a lower PVP concentration and hence a PLGA surface enrichment.

These data concur with the ToF-SIMS results and suggest that the PLGA-rich surface layer comprises at least a thickness of about 10 nm, the depth of analysis for XPS under the conditions used here.

The observed higher experimental atomic carbon concentration for PLGA compared with the theoretical value for the pure polymer suggests a preferential orientation of carbon-rich groups toward the particle surface. Again, the mechanism clarifying this observation is supported by literature, where surface segregation and surface restructuring of the methyl side groups of PLGA have been reported.[22] This statement was evidenced by the C 1s spectrum for spray-dried PLGA that revealed a higher experimental atomic carbon concentration coming from the C—C bond (38.18%) compared with the theoretical value (33.33%), indeed indicating the orientation of methyl groups toward the spray-dried particle surface.

To summarize, for all the investigated samples, regardless of the polymer ratio, the particle shell consists of a PLGA-rich surface layer with an underlying PVP-rich phase. The thickness of this PLGA layer increases with an increasing amount of PLGA present in the sample.

Nanothermal analysis of the samples allows detection of the $T_g$s of the polymer phases at the near surface. As displayed for the PLGA–PVP 40:60 (wt %) sample in Figure 6, not every particle displayed two distinct $T_g$s, often lacking detection of the PLGA shell. The reason that the PLGA shell is not detected for every particle is most likely caused by the fact that for most of the particles the PLGA-rich layer was too thin (and hence of too little mass under the nano-sized probe) for detection with nanoTA. For these particles, an increase in noise in the baseline is observed and can be related to the presence of the PLGA layer (Fig. 6b). This noise is most likely caused by mixing of the thin PLGA surface layer with the underlying PVP phase during heating by the nanoTA tip. The same phenomenon, namely, mixing of the different phases caused by heating, is believed to account for the increased noise observed during the temperature transition of the PVP layer when comparing the sample with the pure polymer.

The discrepancies observed for samples consisting of different PLGA to PVP ratios are a result of the difference in the thickness of the PLGA surface layer. Samples consisting of 80 (wt %) PVP displayed a $T_g$ close to that of pure PVP. As demonstrated before by the $C_{60}^+$ ToF-SIMS sputtering experiment, the thickness of the PLGA-rich surface layer is related to the total amount of PLGA present in the sample. In this case, a sample containing only 20% PLGA had a PLGA surface layer that was too thin for direct detection via a $T_g$ by nanoTA. The same applies to the 40 (wt %) PLGA sample, wherein the detection of the PLGA $T_g$, next to the PVP transition, again depended on the thickness of the PLGA surface layer. For samples containing 80 (wt %) PLGA, the observed transition temperature of about 10°C higher than the one of the pure PLGA can be explained by the presence of a relatively thick PLGA shell containing some PVP, in which case the PVP present in the sample delays the transition temperature by roughly 10°C.

## CONCLUSIONS

Spray drying a feed solution containing PLGA and PVP results in hollow shell-structured microparticles. MDSC proved that two different amorphous phases are present in the particles: a PLGA-rich phase containing some PVP and a PVP-rich phase containing some PLGA.

Scanning electron microscopy clarified that particle sphericity increased with increasing PLGA content. It was observed that surface roughness varied in a range of 20 nm and some interparticle differences are observed, which are assigned to the nature of the spray drying process. The PLGA-rich phase appeared to be the surface layer of the particles, with an underlying PVP-rich layer. This finding was supported by the results of ToF-SIMS, XPS as well as nanoTA experiments.

The polymer ratio has an influence on the thickness of the PLGA surface layer: the higher the weight percentage PLGA present in the sample, the thicker its surface layer is. These findings have implications for the development of the polymeric drug matrix to deliver the optimum drug release properties in future studies.

## ACKNOWLEDGMENTS

P. Rombaut is acknowledged for his general technical support. E. F. Smith is recognized for performing the XPS experiments.

## REFERENCES

1. Baert L, Van 't Klooster G, Dries W, François M, Wouters A, Basstanie E, Iterbeke K, Stappers F, Stevens P, Schueller L, Van Remoortere P, Kraus G, Wigerinck P, Rosier J. 2009. Development of a long-acting injectable formulation with nanoparticles of rilpivirine (TMC278) for HIV treatment. Eur J Pharm Biopharm 72:502–508.
2. Janssens S, Van den Mooter G. 2009. Physical chemistry of solid dispersions. J Pharm Pharmacol 61:1571–1586.
3. Murdande SB, Pikal MJ, Shanker RM, Bogner RH. 2010. Solubility advantage of amorphous pharmaceuticals, part 1: Thermodynamic analysis. J Pharm Sci 99: 1254–1264.
4. Van den Mooter G. 2012 The use of amorphous solid dispersions: A formulation strategy to overcome poor solubility and dissolution rate. Drug Discov Today (in press).
5. Hancock BC, Zografi G. 1997. Characteristics and significance of the amorphous state in pharmaceutical systems. J Pharm Sci 86:1–12.
6. Tran PH, Tran TT, Park JB, Lee BJ. 2011. Controlled release systems containing solid dispersions: Strategies and mechanisms. Pharm Res 28:2353–2378.
7. Mohamed F, Van der Walle CF. 2008. Engineering biodegradable polyester particles with specific drug targeting and drug release properties. J Pharm Sci 97:71–87.
8. Jalil R, Nixon JR. 1990. Biodegradable poly(lactic acid) and poly(lactide-co-glycolide) microcapsules: Problems associated with preparative techniques and release properties. J Microencapsul 7:297–325.
9. Twaites B, de las Heras Alarcón C, Alexander C. 2005. Synthetic polymers as drugs and therapeutics. J Mater Chem 15:441–455.
10. Rhee YS, Sohn M, Woo BH, Thanoo BC, Deluca PP, Mansour HM. 2011. Sustained-release delivery of octreotide from biodegradable polymeric microspheres. AAPS PharmSciTech 12:1293–1301.
11. Eerdekens M, Van Hove I, Remmerie B, Mannaert E. 2004. Pharmacokinetics and tolerability of long-acting risperidone in schizophrenia. Schizophr Res 70:91–100.
12. Wu M, Kleiner L, Tang FW, Hossainy S, Dacies MC, Roberts CJ. 2010. Surface characterization of poly(lactic acid)/everolimus and poly(ethylene vinyl alcohol)/everolimus stents. Drug Deliv 17:376–384.
13. Weuts I, Van Dycke F, Voorspoels J, De Cort S, Stokbroekx S, Leemans R, Brewster ME, Xu D, Segmuller B, Turner YT, Roberts CJ, Davies MC, Qi S, Craig DQ, Reading M. 2011. Physicochemical properties of the amorphous drug, cast films, and spray dried powders to predict formulation probability of success for solid dispersions: Etravirine. J Pharm Sci 100:260–274.
14. Qi S, Belton P, Nollenberger K, Gryczke A, Craig DQ. 2011. Compositional analysis of low quantities of phase separation in hot-melt-extruded solid dispersions: A combined atomic force microscopy, photothermal Fourier-transform infrared microspectroscopy, and localised thermal analysis approach. Pharm Res 28:2311–2326.
15. Fischer GL, Belu AM, Mahoney CM, Wormuth K, Sanada N. 2009. Three dimensional time-of-flight secondary ion mass spectrometry imaging of a pharmaceutical in a coronary stent coating as a function of elution time. Anal Chem 81:9930–9940.
16. Scoutaris N, Hook AL, Gellert PR, Roberts CJ, Alexander MR, Scurr DJ. 2012. ToF-SIMS analysis of chemical heterogeneities in inkjet micro-array printed drug/polymer formulations. J Mater Sci: Mater Med 23:385–391.
17. Galop M. 2005. Study of pharmaceutical solid dispersions by microthermal analysis. Pharm Res 22:293–302.
18. Zhang J, Bunker M, Parker A, Madden-Smith CE, Patel N, Roberts CJ. 2010. The stability of solid dispersions of felodipine in polyvinylpyrrolidone characterized by nanothermal analysis. Int J Pharm 414:210–217.
19. Chen X, Roberts CJ, Zhang J, Davies MC, Tendler SJB. 2002. Phase contrast and attraction-repulsion transition in tapping mode atomic force microscopy. Surf Sci 519:L593–L598.
20. Zhang J, Bunker M, Chen X, Parker AP, Patel N, Roberts CJ. 2009. Nanoscale thermal analysis of pharmaceutical solid dispersions. Int J Pharmaceut 380:170–173.
21. Vehring R. 2008. Pharmaceutical particle engineering via spray drying. Pharm Res 25:999–1022.
22. Bolten D, Türk M. 2011. Experimental study of the surface tension, density and viscosity of aqueous poly(vinlylpyrrolidone) solutions. J Chem Eng Data 56:582–588.
23. Noskov BA, Akentiev AV, Miller R. 2002. Dynamic surface properties of poly(vinylpyrrolidone) solutions. J Colloid Interface Sci 255:417–424.
24. Shard AG, Davies MC, Li YX, Volland C, Kissel T. 1997. XPS and SSIMS analysis revealing surface segregation and short-range order in solid films of block copolymers of PEO and PLGA. Macromolecules 30:3051–3057.
25. Opdahl A, Phillips RA, Somorjai GA. 2002. Surface segregation of methyl side branches monitored by sum frequency geeneration (SGF) vibrational spectroscopy for a series of random poly(ethylene-co-propylene) copolymers. J Phys Chem B 106:5212–5220.
26. Wang J, Woodcock SE, Buck SM, Chen C, Chen Z. 2001. Different surface restructuring behaviors of poly(methacrylate)s detected by SGF in water. J Am Chem Soc 123:9470–9471.
27. Thanki P, Dellacherie E, Six JL. 2006. Surface characteristics of PLA and PLGA films. Appl Surface Sci 253:2758–2764.